DOI: https://doi.org/10.24425/amm.2025.156263

A.S. SANGAR<sup>©1,2</sup>, N.I.M. NADZRI<sup>©1,2\*</sup>, M.F.M. NAZERI<sup>©2</sup>, Y. PUTTHISIGAMANY<sup>©3</sup>, D.S. CHE HALIN<sup>©1,2</sup>, S. JOSEPH<sup>©4</sup>, K. JEŻ<sup>©5</sup>

# COMPARATIVE ANALYSIS OF MICROSTRAIN AND DISLOCATION IN CoCrFeMnNi AND CoCrFeMnNiTi HIGH ENTROPY ALLOYS

Microstrain and dislocation density are critical determinants affecting crystalline materials' mechanical and physical properties. This investigation assesses the changes present in CoCrFeMnNi and CoCrFeMnNiTi high-entropy alloys (HEAs) through the application of X-ray diffraction (XRD) and the Williamson-Hall method for microstrain and dislocation density. Field Emission Scanning Electron Microscope (FESEM)is used for microstructure analysis. It is observed that the transition from the face-centered cubic (FCC) to body-centered cubic (BCC) phase from CoCrFeMnNi to CoCrFeMnNiTi HEA results in a significant shift of the peak towards a lower  $2\theta$  angle by  $0.62^\circ$ . A 30% reduction in microstrain and a 17.49% decrease in dislocation density were noted with the addition of titanium (Ti), which correlated to an increase in hardness measurement of  $952 \pm 5$  HV in CoCrFeMnNiTi. The results indicate the role of Ti in defect dynamics, which is crucial for optimizing material properties.

Keyword: Microstrain; Dislocation density; HEA; Titanium; Structure

#### 1. Introduction

High-entropy alloys (HEAs) represent a significant advancement in material science, having special compositions consisting of several elements that which is nearly in equiatomic ratios [1]. HEAs are unique due to a single phase with more than five elements, whereas conventional alloy typically can made up of one or two elements only [2,3]. HEAs are often found to exhibit rather simple lattices such as body-centered cubic (BCC), face-centered cubic (FCC), or hexagonal closepacked (HCP) with a disordered atom across crystallographic sites [4]. This special arrangement of atoms yields extraordinary properties like high strength, corrosion resistance, and thermal stability, which makes this HEA highly suitable for advanced applications [5]. Microstrain and dislocation density are important parameters of the X-ray diffraction (XRD) peak broadening analysis. Microstrain can be defined as the changes in the lattice deformation caused by crystal defects and dislocations, whereas dislocation density measures the amount of line defects in a crystal structure. Models such as the WilliamsonHall (W-H), Modified W-H (MW-H), and Halder-Wagner use XRD data to identify the effects of crystallite size and strain on line broadening [6-8].

Studies on CoCrFeNi-based HEAs have found significant enhancements in hardness and strength through structural change via alloying. Research on aluminum and molybdenum has demonstrated enhancement of specific properties such as wear resistance and thermal stability [9,10]. Titanium (Ti)-based alloys usually have higher strength, low weight, and high corrosion resistance. This allows Ti-based alloys to be used in various applications such as aerospace, automobile, and chemical plants [11]. Besides, Ti addition has profoundly impacted the microstructure and mechanical properties. Studying CoCrFeMnNiTi<sub>x</sub> alloys synthesized by selective laser melting shows that the addition of Ti induces the formation of intermetallic phases. This is said to yield a noticeable increase in hardness and wear resistance, even if ductility is reduced with an increase in Ti ratios [12]. Similarly, vacuum arc-melted CoCrFeMnNiTi<sub>x</sub> alloys exhibited a phase transition from FCC to BCC as the Ti-content increased, resulting in improved microhardness and tensile strength [13].

Corresponding author: izzatinadzri@unimap.edu.my



<sup>1</sup> UNIVERSITI MALAYSIA PERLIS (UNIMAP), CENTRE OF EXCELLENCE GEOPOLYMER AND GREEN TECHNOLOGY (CEGEOGTECH), FACULTY OF CHEMICAL ENGINEERING

TECHNOLOGY, TAMAN MUHIBBAH, 02600, ARAU, PERLIS, MALAYSIA

UNIVERSITI MALAYSIA PERLIS (UNIMAP), FACULTY OF CHEMICAL ENGINEERING AND TECHNOLOGY, KOMPLEKS PUSAT PENGAJIAN JEJAWI 2, TAMAN MUHIBBAH, 02600 JEJAWI, ARAU, PERLIS, MALAYSIA

<sup>&</sup>lt;sup>3</sup> UNIVERSITI KEBANGSAAN MALAYSIA, SOLAR ENERGY RESEARCH INSTITUTE (SERI), 43600 BANGI, SELANGOR, MALAYSIA

DEPARTMENT OF MATERIALS ENGINEERING, CAMBRIDGE INSTITUTE OF TECHNOLOGY, BENGALURU, KARNATAKA 560036, INDIA

CZESTOCHOWA UNIVERSITY OF TECHNOLOGY, FACULTY OF CIVIL ENGINEERING, 3 AKADEMICKA STR., 42-218 CZESTOCHOWA, POLAND

Recent studies show that  $CrCuFeNi_2Ti$  HEA has BCC structure with  $Ni_3T_i$  intermetallic compound and  $Ti_{0.5}$  has the highest mechanical strength which supports the influence of Ti in the HEA-based alloys [14].

Ti doping in CoCrFeMnNi attracts significant interest due to its potential to enhance the properties of the HEA. However, there is a lack of in-depth studies on the microstrain and dislocation density that occurs upon the addition of Ti. Previous studies have explored XRD results for the phase transition and structural properties. This research addresses this gap by focusing mainly on the microstrain and dislocation density and their effect on the mechanical property of CoCrFeMnNi after adding Ti. In this paper, a comprehensive correlation between the microstrain and dislocation density in CoCrFeMnNi with the addition of Ti has been studied using the application of XRD and the W-H method.

### 2. Experimental procedure

CoCrFeMnNi and CoCrFeMnNiTi ingots with equimolar composition were produced using vacuum melting. The samples were remelted three times to ensure a uniform microstructure and then poured into a mold for casting. The resulting ingots were then cut into smaller cubes of dimensions: of 1 cm  $\times$  1 cm  $\times$  1 cm. The samples were ground using abrasive papers with grit sizes of 180, 600, 800, 1200, and 2000, and polished with 1-micron alumina powder in preparation for testing. Phase analysis was conducted using an X-ray diffractometer (XRD, Bruker AXS-D8) with diffraction angles ranging from 20° to 120°, step-size 0.02°, employing a Cu-K $\alpha$  source ( $\lambda = 1.5406 \text{ Å}$ ). The diffraction peak data was analyzed using HighScore Plus software. The crystallite size (D) was calculated using the equation (1) and Scherrer constant (0.9) with the X-ray wavelength ( $\lambda$ ) (0.15406 nm). The microstrain ( $\varepsilon$ ) and dislocation density ( $\delta$ ) were calculated using equations (2) and (3) derived from the W-H method [15]:

$$D = \frac{0.9 \times \lambda}{\beta \times \cos \theta} \tag{1}$$

$$\varepsilon = \left(\frac{FWHM \left(Rad\right)}{4 \operatorname{Tan}\left(\frac{\pi\theta}{180}\right)}\right)^{2} \tag{2}$$

$$\delta = \frac{1}{\frac{FWHM(Rad)}{4 \operatorname{Tan}\left(\frac{\pi\theta}{180}\right)}}$$
 (3)

where: Full-width-half-maximum (*FWHM*) ( $\beta$ ) is the width of the XRD peak at half of its maximum intensity [radian];  $\theta$  is the Bragg angle [°].

Surface morphology was examined using a FEI Nova Nanosem 450 Field Emission Scanning Electron Microscope (FESEM). The grain size was calculated using the line intercept method ( $\ell$ ) and grain size number calculated using ASTM G, equations (4) and (5) [16]:

$$\ell = \frac{L}{M \times N} \tag{4}$$

$$G = -3.288 - 6.643856 \times \log \ell \tag{5}$$

Where L is the total length of test patterns ( $\mu$ m), M is the magnification used, N is the number of interceptions to the grain boundary. The hardness of the samples was measured at room temperature using an INNOVATEST model 700AS microhardness tester with a load of 1000 gf and a dwell time of 10 seconds.

#### 3. Results and discussion

# 3.1. Phase and structural analysis

Fig. 1 shows the XRD patterns of the CoCrFeMnNi and CoCrFeMnNiTi. In the XRD pattern for both CoCrFeMnNi and CoCrFeMnNiTi, a crystalline structure is observed. Co-CrFeMnNi exhibits three distinct diffraction peaks at 43.65°, 50.82°, and 74.73°, corresponding to the (111), (200), and (220) planes, respectively. These peaks indicate a single FCC crystal structure, as supported by JCPDS card No. 00-065-0528 belonging to the CoCrFeMnNi crystal structure. Upon the addition of Ti, new diffraction peaks appear at 41.04°, 43.03°, 45.27°, and 52.22°, corresponding to the (400), (411), (420), and (431) crystal orientations, respectively. These newly formed peaks signify the development of a BCC crystal structure of CrFeNiTi, as supported by JCPDS card No. 01-081-4958. The main peak angle shifts from 43.65° to 43.03°, a decrease of approximately 0.62° to a lower angle. This peak is in agreement with previous studies conducted by [13].

This shift occurs due to a slight increase in the d-spacing from 2.07 nm in CoCrFeMnNi to 2.08 nm in CoCrFeMnNiTi.

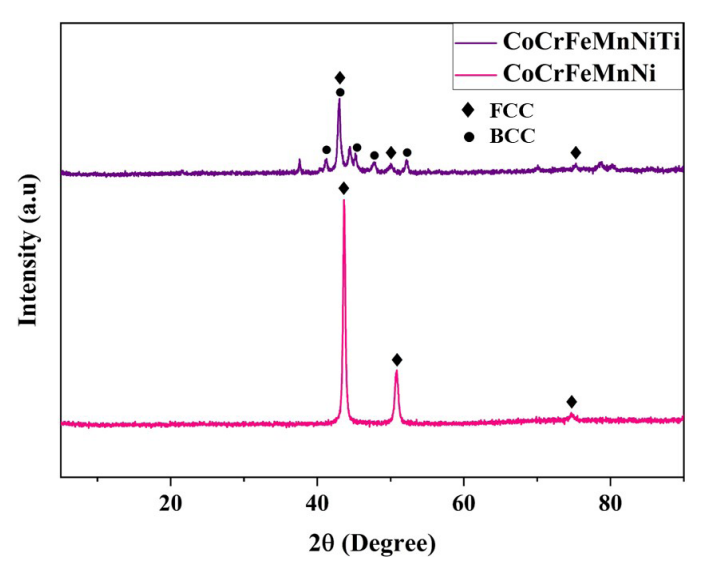


Fig. 1. XRD graph for CoCrFeMnNi and CoCrFeMnNiTi

This increase is attributed to the solid solution effect caused by the addition of larger Ti atoms into the CoCrFeMnNi matrix [17].

The emergence of this BCC phase is due to lattice distortion caused by the larger atomic size and higher lattice parameter of Ti compared to the other elements in CoCrFeMnNi [18,19]. Consequently, the addition of Ti alters the crystal structure of the alloy from a pure FCC phase to a combination of FCC and BCC phases. This observation aligns with the findings in [13]. In addition, the intensity of the main peak of FCC from CoCrFeMnNi has been reduced after adding Ti.

The crystallite size of CoCrFeMnNi was 24.06 nm, whereas for CoCrFeMnNiTi was 29.88 nm. There is an increase of about 24.19% in the crystallite size after the addition of Ti which correlates with the XRD diffraction of the main peak has a lower intensity and is much broader.

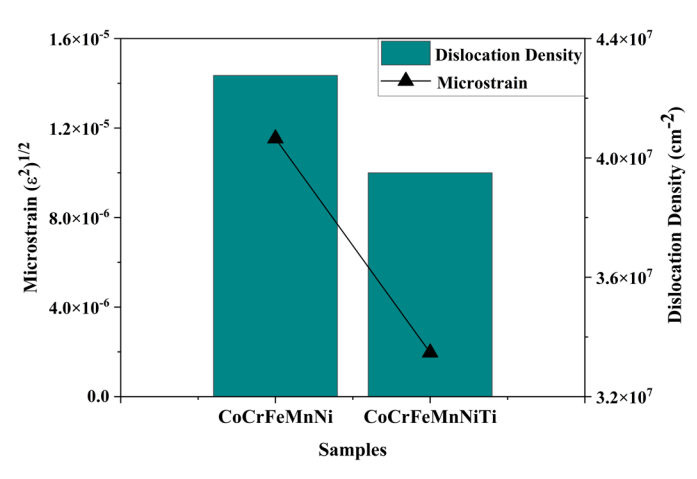


Fig. 2. Microstrain and dislocation density values for CoCrFeMnNi and CoCrFeMnNiTi

This is due to the changes in the phase from FCC to BCC. BCC structure typically has a less densely packed structure compared to FCC as shown in Fig. 3 which allows more space for crystal growth [20]. In addition, both microstrain and dislocation density have been reduced (Fig. 2) after the addition of Ti. There is a reduction of approximately 30% in microstrain and 17.49% in dislocation density respectively. Ti has a larger atomic radius compared to constituent atoms in the CoCrFeMnNi HEA. Thus, Ti doping will cause lattice expansion leading to a redistribution of internal stress that reduces lattice distortion and microstrain [21]. This reduction correlates with increased crystallite size and lattice constant [22].

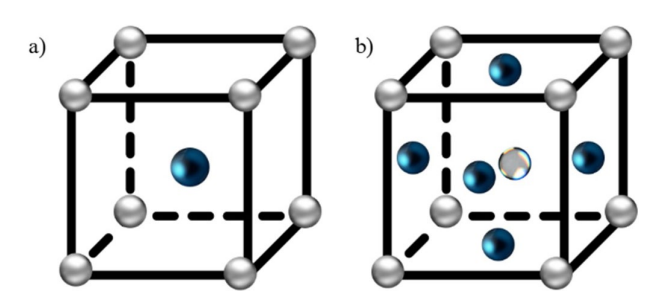
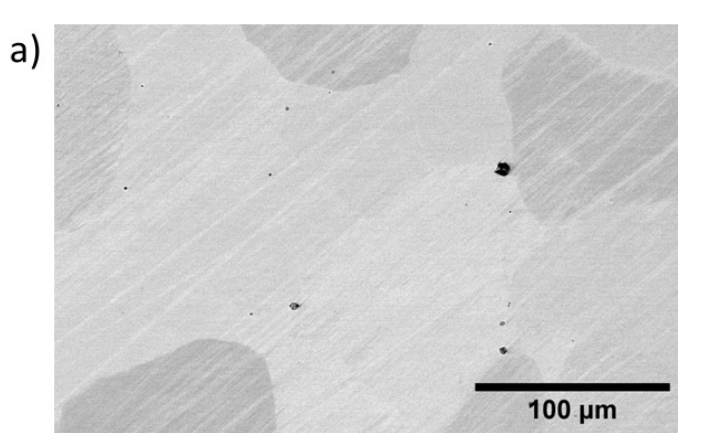


Fig. 3. Body-centered cubic (BCC) and face-centered cubic (FCC) crystal structure

### 3.2. Surface morphology

The microstructural analysis of CoCrFeMnNi and CoCrFeMnNiTi HEAs, conducted using FESEM, has been shown in Fig. 4. In the CoCrFeMnNi HEA, contrast variations across the microstructure indicate distinct elemental concentrations and phase distributions. Upon adding Ti, the CoCrFeMnNiTi HEA shows the emergence of a new Ti-rich phase, uniformly distributed in non-uniform, island-like formations. Additionally, the microstructure of CoCrFeMnNiTi HEA exhibits a dendritic structure interspersed with irregular island grains as confirmed by other scholars [13,23]. The lamella structure is characterized by alternating dark and light lines. This is caused by the precipitation of Ti that produces lamella structure.



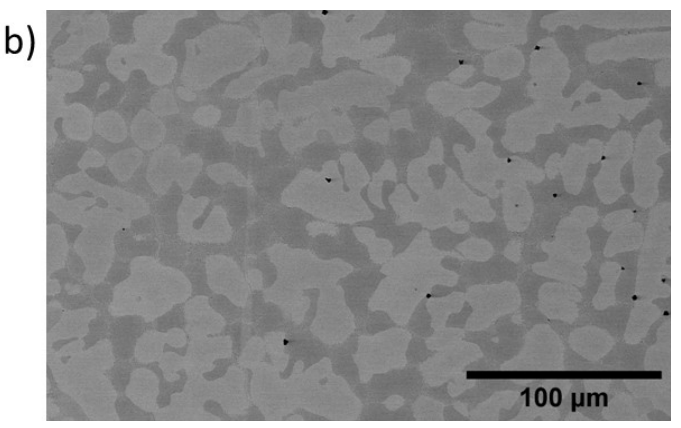


Fig. 4. Microstructure of a) CoCrFeMnNi, b) CoCrFeMnNi with Ti addition HEA

Fig. 5 shows the average grain size for CoCrFeMnNi and CoCrFeMnNiTi. The darker grains  $(9.09\times10^{-3}~\mu\text{m})$  are smaller compared to lighter grains  $(12.13\times10^{-3}~\mu\text{m})$  for CoCrFeMnNi. However, after the addition of Ti darker grains  $(2.55\times10^{-3}~\mu\text{m})$  are bigger compared to lighter grains  $(2.02\times10^{-3}~\mu\text{m})$ . A comparison of the percentage differences in grain size highlights the significant effect of Ti doping. The darker grains decrease in size by 71.43%, while the lighter grains exhibit a striking 83.31% reduction after adding Ti. The grain size number for CoCrFeMnNi darker grains  $(10.30~\mu\text{m})$  and lighter grains  $(9.45~\mu\text{m})$  while for CoCrFeMnNiTi darker grains  $(13.89~\mu\text{m})$  and lighter grains  $(14.64~\mu\text{m})$  respectively.

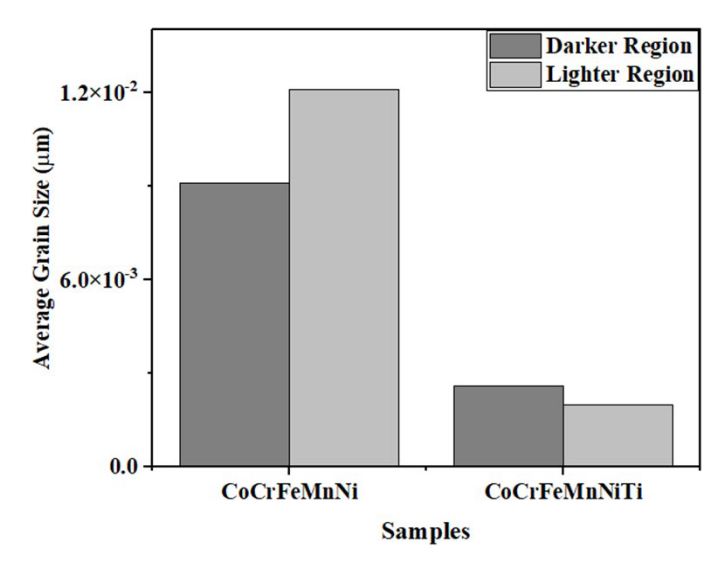


Fig. 5. The average grain size (%) in CoCrFeMnNi and CoCrFeMnNiTi for darker and lighter regions

The grain size number is inversely proportional to the average grain size. The larger the grain size number, the smaller the average grain size in the microstructure [16]. This substantial reduction in grain size is due to the larger atomic size of Ti and its distinct chemical affinity compared to the other elements, which induces phase segregation during solidification. As Ti precipitates, it hinders grain growth, leading to the formation of these smaller grains [24].

### 3.2. Mechanical properties

The Vickers microhardness values of the CoCrFeMnNi and CoCrFeMnNiTi HEAs are presented in TABLE 1. The CoCrFe MnNiTi exhibits a significantly higher hardness of 952±5 HV, compared to CoCrFeMnNi with a hardness of 157±5 HV. Incorporating Ti atoms into the CoCrFeMnNi HEA increases the lattice parameters. It causes lattice distortion within the facecentered cubic (FCC) structure, which impedes dislocation movement and enhances the resistance of alloy to deformation [13].

TABLE 1 Microhardness values for CoCrFeMnNi and CoCrFeMnNiTi

| Samples      | Reading    |
|--------------|------------|
| CoCrFeMnNi   | 157 ± 5 HV |
| CoCrFeMnNiTi | 952 ± 5 HV |

The addition of Ti enhances the strength of the CoCrFeMn-NiTi HEA through multiple mechanisms, including solid solution strengthening, dislocation strengthening, and precipitation [24]. The modification of FCC structure to BCC due to the addition of Ti introduced a reduced quantity of slip systems which caused the hardness to increase [19]. In addition, the reduction in both microstrain and dislocation density causes a reduction in the number of mobile dislocations. This can contribute to plastic deformation and enhance the material's ability to resist stress under an applied force [25]. Moreover, a decrease in microstrain reduces the availability of slip systems and reduces the dislocation movement [26]. Apart from that, the microstructure shows Ti precipitation, forming a lamellar structure that contributes to the overall hardness. Furthermore, the dendritic structure imparts a brittle characteristic to the material, further increasing its hardness. The smaller grain size also causes the hardness to increase in CoCrFeMnNiTi [27]. Thus, the observed increase in hardness is primarily attributed to dislocation and precipitation strengthening.

#### 4. Conclusion

This paper reports on a comparative study of microstrain and dislocation density of CoCrFeMnNi and CoCrFeMnNiTi. XRD patterns show that the addition of Ti leads to a peak shift to a low angle and causes changes in structure from FCC to BCC. With the addition of Ti, microstrain and dislocation density decreased, while crystallite size and lattice parameters increased. Moreover, the microhardness measurement indicated that the Ti-enhanced CoCrFeMnNi had a value of 952±5 HV, which was significantly higher. This improvement is due to the phase evolution of CoCrFeMnNiTi from FCC to BCC. Furthermore, the decrease in microstrain hinders the movement of dislocations, which elevates resistance to greater stress. Ti addition also influences the microstructure by producing a dendritic structure and smaller grain size. Overall, Ti addition has a beneficial effect on the CoCrFeMnNi-HEA phase and its structure.

#### Acknowledgments

The authors would like to acknowledge that the study covered in this manuscript was funded by the Ministry of Higher Education Malaysia on the financial support under grant reference no: FRGS/1/2022/STG05/ UNIMAP/02/3.

## REFERENCES

- [1] S.-Y. Park, J. Pyo Park, K.-A. Lee, Microstructure and Wear Property of In-Situ Oxide Reinforced CrMnFeCoNi High Entropy Alloy Composite Fabricated by Selective Laser Melting. Arch. Metall. Mater. 69, 447-452 (2024).
  - DOI: https://doi.org/10.24425/amm.2024.149764
- R. Bureš et al., FeSiBAlNiMo high entropy alloy prepared by mechanical alloying. Acta Phys. Pol. A, 131 (4), 771-773 (2017). DOI: http://doi.org/10.12693/APhysPolA.131.771
- A.A. Akinwande, O.A. Balogun, A.A. Adediran, O.S. Adesina, V. Romanovski, T.C. Jen, Experimental analysis, statistical modeling, and parametric optimization of quinary-(CoCrFeMnNi)<sub>100-x</sub>/ TiCx high-entropy-alloy (HEA) manufactured by laser additive manufacturing. Results Eng. 17, 100802 (2023). DOI: https://doi.org/10.1016/j.rineng.2022.100802

- [4] K. Jasiewicz, S. Kaprzyk, J. Tobola, Interplay of crystal structure preference and magnetic ordering in high entropy CrCoFeNiAl alloys. Acta Phys. Pol. A, 133 (3), 511-513 (2018). DOI: http://doi.org/10.12693/APhysPolA.133.511
- [5] M.S. Kim, H.S. Son, G.S. Joo, Y.D. Kim, H.J. Choi, S.H. Kim, Fabrication of Aluminum Matrix Composite Reinforced with Al 0.5 CoCrCuFeNi High-Entropy Alloy Particles. Arch. Metall. Mater. 67 (4), 1543-1546 (2022). DOI: https://doi.org/10.24425/amm.2022.141091
- [6] B. Himabindu, N.L. Devi, B.R. Kanth, Microstructural parameters from X-ray peak profile analysis by Williamson-Hall models; A review. Mater. Today-Proc. 47 (14), 4891-4896 (2021). DOI: https://doi.org/10.1016/j.matpr.2021.06.256
- [7] A. Borbély, The modified Williamson-Hall plot and dislocation density evaluation from diffraction peaks. Scripta Mater. 217 (3), 114768 (2022).
  - DOI: https://doi.org/10.1016/j.scriptamat.2022.114768
- [8] A.S. Abdel-Rahman, Y.A. Sabry, An approach to the micro-strain distribution inside nanoparticle structure. Int. J. Nonlin. Mech. 161, 104670 (2024).
  - DOI: https://doi.org/10.1016/j.ijnonlinmec.2024.104670
- [9] Z. Wu et al., Review on the Tensile Properties and Strengthening Mechanisms of Additive Manufactured CoCrFeNi-Based High-Entropy Alloys. Metals-Basel 14 (4), 437 (2024). DOI: https://doi.org/10.3390/met14040437
- [10] P. Müller, A. Zadera, L. Čamek, M. Myška, V. Pernica, Metallurgical Processing of CoCrFeNi High-Entropy Alloy. Archives of Foundry Engineering 24, 56-62 (2024).
  DOI: http://doi.org/10.24425/afe.2024.151310
- [11] G. Prabu, M. Duraiselvam, Tribological studies on AlCrFeCu-CoNi high entropy alloy surface coated on Ti-6Al-4V using plasma transferred arc technique. Arch. Metall. Mater. 67 (2) 409-420 (2022).
  - DOI: https://doi.org/10.24425/amm.2022.137772
- [12] C. Bulut, F. Yıldız, T. Varol, T.O. Ergüder, Effect of titanium on the structural, mechanical and surface properties of CoCrFeMn-NiTi<sub>x</sub> high entropy alloy fabricated by selective laser melting. Intermetallics 169, 108281 (2024). DOI: https://doi.org/10.1016/j.intermet.2024.108281
- [13] Y. Chen et al., Effect of Ti content on the microstructure and properties of CoCrFeNiMnTi<sub>x</sub> high entropy alloy. Entropy **24** (2), 241 (2022). DOI: https://doi.org/10.3390/e24020241
- [14] L. Chen, Microstructure Evolution, Phase Composition, Tensile and Hardness Properties Investigation of CrCuFeNi<sub>2</sub>Ti<sub>x</sub>-Based High-Entropy Alloys. Arch. Metall. Mater. 68 (3), 881-886 (2023). DOI: https://doi.org/10.24425/amm.2023.145451
- [15] M. Rabiei et al., X-ray diffraction analysis and Williamson-Hall method in USDM model for estimating more accurate values of Stress-Strain of unit cell and super cells (2×2×2) of hydroxyapatite, confirmed by Ultrasonic Pulse-Echo Test. Materials **14** (11), 2949 (2021).
  - DOI: https://doi.org/10.3390/ma14112949

- [16] X. Li et al., Automation of intercept method for grain size measurement: A topological skeleton approach. Mater. Design **224** (9), 111358 (2022).
  - DOI: https://doi.org/10.1016/j.matdes.2022.111358
- [17] L. Zhang et al., Titanium doping levels and their effects on FeCo-CrNi high-entropy alloys: From microstructure to performance. Mater. Charact. 215, 114136 (2024).
  - $DOI: \ https://doi.org/10.1016/j.matchar. 2024. 114136$
- [18] M. Karimzadeh, M. Malekan, H. Mirzadeh, L. Li, N. Saini, Effects of titanium addition on the microstructure and mechanical properties of quaternary CoCrFeNi high entropy alloy. Mat. Sci. Eng. A-Struct. 856 (6), 143971 (2022).
  DOI: https://doi.org/10.1016/j.msea.2022.143971
- [19] Y.-C. Hsu, C.-L. Li, C.-H. Hsueh, Effects of Al addition on microstructures and mechanical properties of CoCrFeMnNiAl<sub>x</sub> high entropy alloy films. Entropy **22** (1), 2 (2019).
  - DOI: https://doi.org/10.3390/e22010002
- [20] S. S. Yadav, R. Dhiman, R. M. Anklekar, Mater. Sci. Eng. Cambridge Scholars Publishing (2024).
- [21] P.-Y. Chen, C.-H. Hsueh, Effects of Ti addition and annealing on microstructure and mechanical properties of CoCrFeMnNi highentropy alloy. J. Mater. Sci. 59 (23), 10526-10540 (2024). DOI: http://doi.org/10.1007/s10853-024-09790-3
- [22] A. Begum, A. Hussain, A. Rahman, Effect of deposition temperature on the structural and optical properties of chemically prepared nanocrystalline lead selenide thin films. Beilstein J. Nanotech. 3 (1), 438-443 (2012).
  - DOI: https://doi.org/10.3762/bjnano.3.50
- [23] J. Wang, B. Zhang, Y. Yu, Z. Zhang, S. Zhu, Z. Wang, Ti content effect on microstructure and mechanical properties of plasmacladded CoCrFeMnNiTi<sub>x</sub> high-entropy alloy coatings. Surface Topography: Metrology and Properties 8 (1), 015004 (2020). DOI: http://doi.org/10.1088/2051-672X/ab615b
- [24] S.J. Brito-Garcia, J.C. Mirza-Rosca, C. Jimenez-Marcos, I. Voiculescu, Impact of Ti doping on the microstructure and mechanical properties of CoCrFeMoNi high-entropy alloy. Metals-Basel 13 (5), 854 (2023).
  - DOI:https://doi.org/10.3390/met13050854
- [25] L. Cui, S. Jiang, J. Xu, R.L. Peng, R.T. Mousavian, J. Moverare, Revealing relationships between microstructure and hardening nature of additively manufactured 316L stainless steel. Mater. Design 198, 109385 (2021).

DOI: https://doi.org/10.1016/j.matdes.2020.109385

- [26] P. Strunz, L. Kunčická, P. Beran, R. Kocich, C. Hervoches, Correlating microstrain and activated slip systems with mechanical properties within rotary swaged WNiCo pseudoalloy. Materials 13 (1), 208 (2020).
  DOI: https://doi.org/10.3390/ma13010208
- [27] J.-R. Lee et al., Effects of building direction and heat treatment on the local mechanical properties of direct metal laser sintered 15-5 PH stainless steel. Mater. Charact. 167 (6), 110468 (2020). DOI: https://doi.org/10.1016/j.matchar.2020.110468